Optical characterization of 2D heterostructure MoS_2/WS_2 using spectroscopic ellipsometry

Nguyen Hoang Tung*, Le Van Long, Nguyen Thi Mai,
Bui Xuan Khuyen, Nguyen Thi Giang, Nguyen Nhat Linh

Institute of Materials Science, Vietnam Academy of Science and Technology, 18 Hoang Quoc Viet, Cau Giay, Hanoi, Vietnam.
*Corresponding author: tungnh@ims.vast.ac.vn
Received 13 Oct. 2024; Revised 23 Dec. 2024; Accepted 5 Feb. 2025; Published 25 Feb. 2025.
DOI: https://doi.org/10.54939/1859-1043.j.mst.101.2025.117-123

ABSTRACT

TMDC materials like MoS_2 and WS_2 are well known for their unique monolayer properties, ideal for optoelectronic applications. Stacking these monolayers enhances the properties beneficial for light detection and harvesting devices. This study investigates the dielectric function and critical point (CP) energies of heterostructure MoS_2/WS_2 using spectroscopic ellipsometry (SE) within the spectral range of 1.5 to 6.0 eV at different angles. The SE method, employing the Tauc-Lorentz model for detailed analysis, confirms the formation of high-quality TMDC heterostructure and provides precise values for intrinsic properties. These results are crucial for optimizing TMDC-based optoelectronic devices for military and commercial applications.

Keywords: Heterostructure MoS_2/WS_2; Spectroscopic ellipsometry; Tauc-Lorentz model; Optical properties.

1. INTRODUCTION

In recent years, transition-metal dichalcogenides (TMDC) have emerged as a promising new class of semiconductor materials due to their unique monolayer properties [1, 2]. Known as "beyond-graphene", these materials exhibit notable physical and chemical characteristics, such as transitions from indirect to direct semiconductors and enhanced quantum efficiencies when shifting from bulk to monolayer structures [3-5]. Research interest in TMDCs has surged, driven by the ability to stack different monolayers to create heterostructures, which enhances properties through interlayer coupling [6], interlayer charge transfer [7], and Moire patterns [8]. These diverse optoelectronic properties make TMDC heterostructures highly promising for optoelectronic applications, including photodetectors and photovoltaic devices, with potential uses in both military and civilian sectors like infrared imaging [9, 10], missile guidance [11, 12], environmental monitoring [13, 14], optical signal transmission [15], and energy conversion [16, 17].

Among TMDC materials, MoS_2 stands out as one of the most intensively researched, displaying standard TMDC features such as van der Waals layered structures and transitions from indirect to direct bandgaps in monolayers [18]. WS_2 has also gained attention for its high quantum yield in 2D systems and significant spin-orbit coupling characteristics [19]. The vertical stacking of MoS_2 and WS_2 monolayers forms heterostructures with exceptional properties desired in optoelectronic fields, especially for light detection and harvesting [20, 21]. Recent advancements in fabrication techniques have enabled the production of high-quality, uniform monolayers and heterostructures of MoS_2 and WS_2, allowing these materials closer to commercial applications [22]. To fully exploit the potential of TMDC heterostructures, knowledge of their intrinsic optical properties is crucial. Despite extensive studies on monolayer MoS_2 and WS_2 over the past decade, there are only a few reports on the dielectric function and refractive index of these monolayer heterostructures [23-25]. A detailed study of the optical characteristics of the refractive index of heterostructures formed by MoS_2/WS_2 using the SE method is not yet available as far as we know.

In this study, we present the dielectric function and CP energies of heterostructures formed by MoS_2 and WS_2 monolayers measured and investigated using the SE method in the spectral range

from 1.5 to 6.0 eV with varying angles of incidence at 60°, 65°, and 70°. Changing the angle of incidence in SE measurements allows for more accurate analyses, identifying the most precise values of both the real and imaginary parts of the refractive index of the material. The values measured by the SE method are fitted using an air/TMDC heterostructure film/sapphire substrate optical model, where the parameters of the air and sapphire substrate are known, and the optical characteristics of the TMDC heterostructure film are modeled using a linear combination of wavelength-dependent oscillators following the Tauc-Lorentz model to construct the individual oscillators. From this fitting result, the real and imaginary parts of the TMDC heterostructure material are simultaneously obtained without using the Kramers-Kronig relationship, achieving more accurate values. Through the fitting process, the values of critical points in the Brillouin zone are also presented and compared with the results found by X. Zhu et al. [24].

2. EXPERIMENTAL DETAILS

2.1. Theoretical foundations

2.1.1. Optical characterization

The SE measures changes in light's polarization state as it reflects off a sample [26]. The fundamental equation of ellipsometry is the ratio ρ of the Fresnel reflection coefficients for *p* and *s* polarized light (r_p, r_s) as shown in Eq. (1) [27]:

$$\frac{r_p}{r_s} = tan\Psi \exp(i\Delta) = \frac{sin^2\phi - cos^2\phi[< \varepsilon > -sin^2\phi]^{\frac{1}{2}}}{sin^2\phi + cos^2\phi[< \varepsilon > -sin^2\phi]^{\frac{1}{2}}} \quad (1)$$

Since the polarization state changes as light reflects off the sample surface, Ψ is the amplitude ratio for the *s* and *p* polarization types before and after reflection, while Δ indicates the phase shift for these polarization types. Based on Eq. (1), one can determine the sample's thickness, refractive and extinction coefficients at measured energy range. In this work, SE measurements were conducted using the VASE spectroscopic ellipsometer (Woollam Co. Inc., Lincoln, NE, USA). Samples were measured at three incidence angles: 60°, 65° and 70° within the energy range of 1.5 to 6.0 eV. For data analysis, all angular spectra were combined and fitted simultaneously using the WVASE v.3.786 software package.

2.1.2. Tauc-Lorentz model

The Tauc-Lorentz model, integrating the features of both the Tauc and Lorentz models, has been used successfully for decades and on many different semiconductors [28, 29]. The mathematical form of the Tauc-Lorentz model is presented in Eq. (2) for photon energy *E* greater than E_g. In Eq. (2), ε_{2TL} represents the imaginary part of the dielectric function, *A* denotes the transition amplitude, *C* is Lorentz oscillator's broadening, E_0 is the peak position of the Lorentz oscillator, and E_g is the bandgap energy, identified as the photon energy where ε_2 becomes zero. The effects of these parameters on the imaginary part of the dielectric function in the Tauc-Lorentz model are illustrated in figure 1. The real part of the dielectric function, ε_1 (*E*) can be obtained from ε_2 (*E*) using the Kramers–Kronig relationship. Traditionally, this expression is employed to fit optical transmission data near the band gap, assuming the real part of the dielectric function remains constant.

$$\varepsilon_{2TL}(E) = \begin{cases} \frac{AE_0C(E-E_g)^2}{(E^2-E_0^2)^2 + C^2E^2} \times \frac{1}{E} & E > E_g \\ 0 & E < E_g \end{cases} \quad (2)$$

This model is limited that the Tauc-Lorentz expression applies exclusively to interband transitions [30]. It does not account for the dielectric response from infrared transitions, Urbach

tail effects, or core transitions as outlined in Eq. 2. Additionally, the Tauc-Lorentz expression is an empirical model. Here, oscillator expressions are employed to approximate the joint density of states multiplied by an average transition probability matrix element.

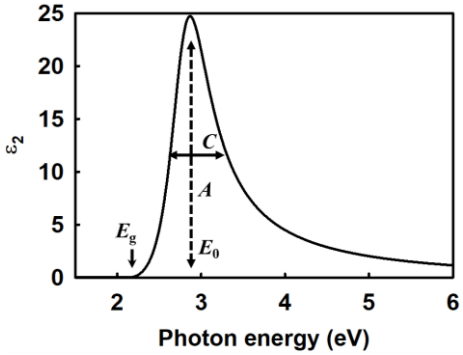

Figure 1. *Effects of Tauc-Lorentz model parameters on the imaginary part.*

3. RESULTS AND DISCUSSION

Heterostructure MoS_2/WS_2 in this work has each monolayer MoS_2 and WS_2 fabricated separately by chemical vapor deposition method and transferred onto each other by standard PMMA method [31]. Figure 2(a) show optical image of the heterostructure taken by Optical Microscope. By color contrast, we can distinguish MoS_2/WS_2 heterostructure and WS_2 monolayer at the edge of the samples. There are some dark and white blurred colors due to reflection of the backside. Figure 2 (b) presents the measured PL spectrum of heterostructure MoS_2/WS_2 in comparison to that of monolayer WS_2. PL intensity of the heterostructure is well quenched due to typical interlayer charge transfer in type II heterojunction [32]. It means the two monolayers are in good contact. It should be noted that, after transferring, the heterostructure was baked in vacuum condition to enhance the interlayer interaction. In Raman data shown in figure 2(c), we marked the vibration modes corresponding to each monolayer. It has been confirmed that Raman vibration of the heterostructure in the region from 300 to 500 cm^{-1} is the superposition of the vibration mode of each constituent monolayer (384 – 405 cm^{-1} for monolayer MoS_2 and 357 – 420 cm^{-1} for monolayer WS_2) [33], this is in good agreement with data reported by X. Zhu et al. (384.7 – 404.1 cm^{-1} for monolayer MoS_2 and 358.0 – 416.5 cm^{-1} for monolayer WS_2) [24]. Therefore, we conclude that our heterostructure MoS_2/WS_2 is in good condition for SE experiment.

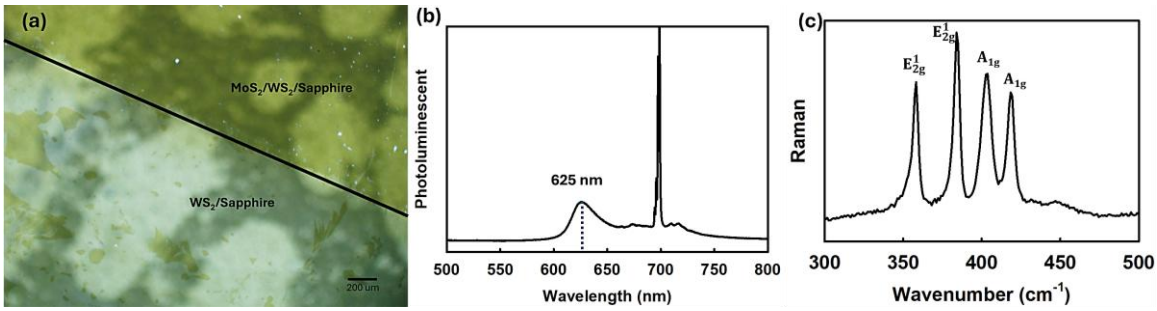

Figure 2. *(a) Optical image, (b) Photoluminescent result and (c) Raman Spectroscopic result of the heterostructre MoS_2/WS_2.*

Figure 3 shows the result of fitting the experimental parameters of Ψ and Δ at three AOIs; the quality of fit is seen to be excellent. For preliminary modelling, the point-by-point fitting approach was applied to obtain a reference dielectric function for the heterostructure [30]. The fitting was conducted at each wavelength based on the assumption that the refractive index and extinction coefficient are linked by the Kramers-Kronig relation, ensuring the model's consistency with

experimental data. Subsequently, the experimental data were parameterized using the Tauc-Lorentz oscillator model. Key parameters characterizing the applied oscillator models, such as the energy gap (E_g), amplitude (*Amp*), broadening parameter (C), and transition point (E_0), are detailed in table 1. The WVASE software employs the Levenberg-Marquardt method to minimize the MSE by adjusting the model fit parameters. The best fit was achieved by adjusting twenty-four parameters listed in table 1, evaluated using the reduced "goodness of fit" criterion. The fitting process yielded a mean square error (MSE) of 2.64, demonstrating that the model accurately represents the data.

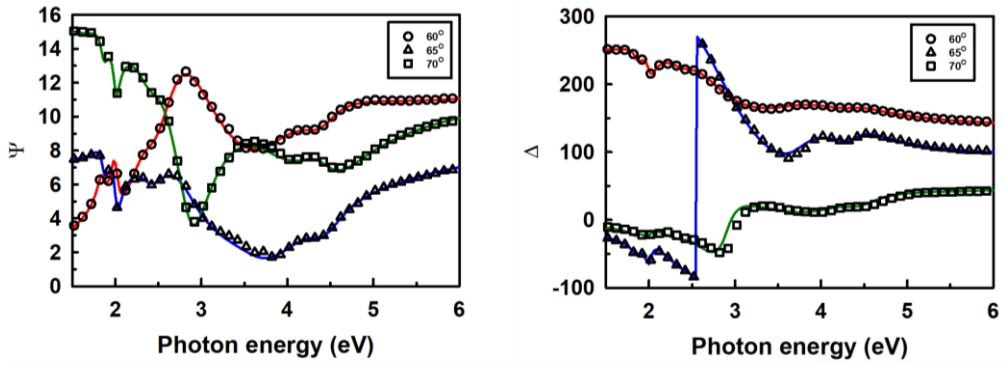

Figure 3. *Experimental and fitting results of Ψ and Δ at angle of incidents 60°, 65°, and 70°. The straight line is the best fit to the data.*

The complex dielectric function at photon energies from 1.5 to 6. eV for the heterostructure layer was deduced by using a multilayer calculation and the result shown in figure 4. The determination of optical E_g is not possible through the application of Lorentz oscillators. Therefore, to determine common E_g, Tauc–Lorentz models were applied. By using each of these models, we could achieve good fitting in the photon energy range of 1.5 to 6.0 eV. In the range from 3 – 4 eV, some discrepancies between the measurement data and the applied models can be noticed. The models used were the simplest possible given the structures and the parameterizations used. That is, no thickness-dependent refractive indices or effective medium approximation interface layers were needed to obtain good fits for the data. Only four parameters in the Tauc-Lorentz model were needed Amp, E_0, C, and E_g. Since spectroscopic ellipsometry generally produces very accurate data, this is a very good indication that the Tauc-Lorentz model works very well in parameterizing the refractive index and extinction coefficient of these films. The band gap parameter from the Tauc-Lorentz model E_g is particularly useful, it can be correlated with chemical and mechanical properties of the films. The ε_2 spectrum for heterostructure MoS_2/WS_2 consists of seven Tauc-Lorentz oscilators with the parameters shown in table 1. Seven CPs found at 1.86, 2.00, 2.39, 2.79, 3.96, 4.55, and 4.83 are in good agreement with the previous work published by X. Zhu et al. [24].

Table 1. *Seven Tauc-Lorentz oscillators with the fitting parameters.*

CPs	Amp	E_0	C	E_g	E_0 (WS_2/MoS_2)*
A	89.02 ± 7.81	1.86 ± 0.02	0.10 ± 0.005	1.72 ± 0.007	1.86
B	104.14 ± 7.36	2.00 ± 0.03	0.09 ± 0.003	1.83 ± 0.009	2.03
C	6.26 ± 1.6	2.39 ± 0.01	0.36 ± 0.012	1.09 ± 0.151	2.28
D	235.01 ± 3.16	2.79 ± 0.02	0.57 ± 0.004	2.13 ± 0.008	2.80
E	75.29 ± 4.16	3.96 ± 0.04	0.56 ± 0.028	3.41 ± 0.027	4.26
F	115.11 ± 6.78	4.55 ± 0.03	0.68 ± 0.030	4.01 ± 0.030	4.50
G	36.52 ± 1.25	4.83 ± 0.05	4.37 ± 0.206	1.10 ± 0.436	4.62

**Data by X. Zhu et al. [24].*

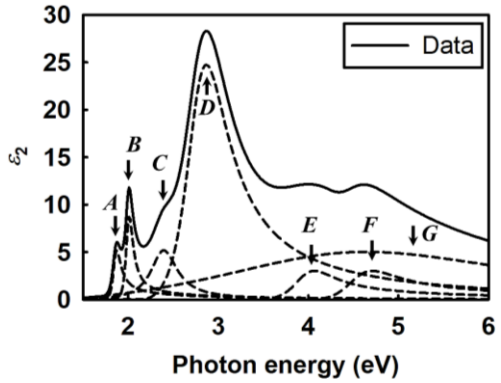

Figure 4. *ε_2 of heterostructure MoS_2/WS_2 is constructed from the Tauc-Lorentz models.*

Below the band gap, the Tauc–Lorentz model provides the best fitting. The imaginary part of ε is represented by the solid line in figure 4. The dashed lines are the Tauc–Lorentz component and structures combined to reconstruct the ε_2 spectrum of heterostructure MoS_2/WS_2. The dashed lines indicate the contributions from each critical point, while the solid line represents their sum. In figure 4, *A*, *B*, *C*, and *D* are exciton transitions in which *A*, *B*, and *C* are from each individual monolayer MoS_2 and WS_2 at K-point in the Brioulin region, while *D* exciton originate from Γ-point transition as a result of combined band structure of the monolayers.

The application of Tauc–Lorentz models allowed us to determine the refractive indices and extinction coefficients of the heterostructure MoS_2/WS_2 within the measured energy range by using the definition of refractive index as

$$n + ik = \sqrt{\varepsilon_1 + i\varepsilon_2} \tag{3}$$

Figure 5 presents the spectral dispersion relations of the refractive index and the extinction coefficient for heterostructure MoS_2/WS_2 by (a) photon energy and (b) wavelength. The region of exciton transition occurs between 1.5 and 3.0 eV.

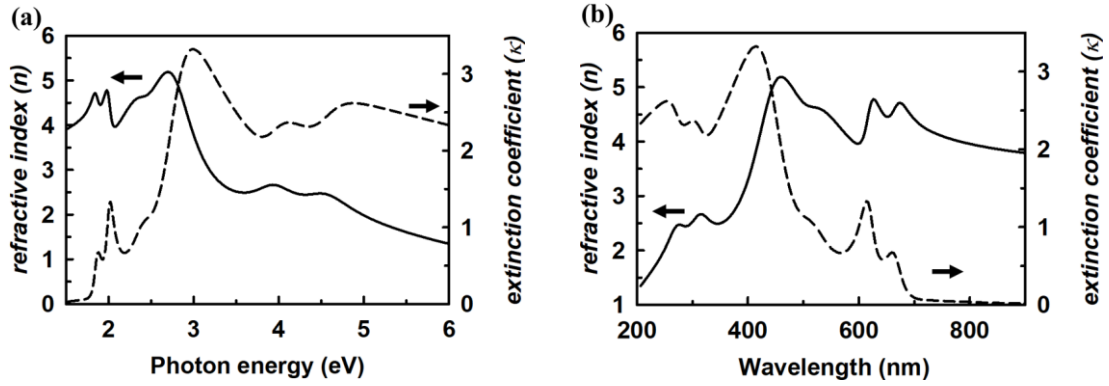

Figure 5. *Dispersion relations of optical constant for heterostructure MoS_2/WS_2 with (a) photon energy and (b) wavelength.*

4. CONCLUSIONS

In this work, SE data of the heterostructure MoS_2/WS_2 at various angles of incidents of 60°, 65°, and 70°. The obtained data have been fit using the Tauc-Lorentz model. The optical constants of the heterostructure MoS_2/WS_2 were extracted as a combination of seven Tauc-Lorentz oscillators corresponding to seven critical point transitions. Optical image, photoluminescence and Raman spectroscopy confirmed the quality of the heterostructure. Besides the determination of complex refractive index, other electronic parameters of the heterostructure (band gap E_g,

transition energy E_0, amplitude A and broadening C) were also reported. The obtained results should be useful for physical understanding and application for optical devices based on embedded 2D heterostructure MoS_2/WS_2.

Acknowledgement: *This research was funded by the Vietnam Academy of Science and Technology, grant number THTETN.05/22-23.*

REFERENCES

[1]. S. Manzeli, et al., *"2D transition metal dichalcogenides",* Nature Reviews Materials, Vol. 2, No. 8, pp. 1-15, (2017).
[2]. A. Chaves, et al., *"Bandgap engineering of two-dimensional semiconductor materials",* npj 2D Materials and Applications, Vol. 4, No. 1, pp. 29, (2020).
[3]. D. Monga, et al., *"Advances in transition metal dichalcogenide-based two-dimensional nanomaterials",* Materials Today Chemistry, Vol. 19, No. pp. 100399, (2021).
[4]. M. Wu, et al., *"Synthesis of two-dimensional transition metal dichalcogenides for electronics and optoelectronics",* InfoMat, Vol. 3, No. 4, pp. 362-396, (2021).
[5]. X. Wu, et al., *"Recent advances on transition metal dichalcogenides for electrochemical energy conversion",* Advanced Materials, Vol. 33, No. 38, pp. 2008376, (2021).
[6]. X. Wu, et al., *"Recent Advances on tuning the interlayer coupling and properties in van Der Waals heterostructures",* Small, Vol. 18, No. 15, pp. 2105877, (2022).
[7]. M.S. Stark, et al., *"Intercalation of layered materials from bulk to 2D",* Advanced Materials, Vol. 31, No. 27, pp. 1808213, (2019).
[8]. F. He, et al., *"Moiré patterns in 2D materials: a review",* ACS nano, Vol. 15, No. 4, pp. 5944-5958, (2021).
[9]. X. Guan, et al., *"Recent progress in short-to long-wave infrared photodetection using 2D materials and heterostructures",* Advanced Optical Materials, Vol. 9, No. 4, pp. 2001708, (2021).
[10]. A. Elbanna, et al., *"2D material infrared photonics and plasmonics",* ACS nano, Vol. 17, No. 5, pp. 4134-4179, (2023).
[11]. H. Li, et al., *"Recent progress and strategies in photodetectors based on 2D inorganic/organic heterostructures",* 2D Materials, Vol. 8, No. 1, pp. 012001, (2020).
[12]. Z. Yan, et al., *"Emerging two-dimensional tellurene and tellurides for broadband photodetectors",* Small, Vol. 18, No. 20, pp. 2200016, (2022).
[13]. X. Chen, C. Liu, and S. Mao, *"Environmental analysis with 2D transition-metal dichalcogenide-based field-effect transistors",* Nano-micro letters, Vol. 12, No. pp. 1-24, (2020).
[14]. D. Tyagi, et al., *"Recent advances in two-dimensional-material-based sensing technology toward health and environmental monitoring applications",* Nanoscale, Vol. 12, No. 6, pp. 3535-3559, (2020).
[15]. M.S. Rahman and L.F. Abdulrazak, *"Utilization of a phosphorene-graphene/TMDC heterostructure in a surface plasmon resonance-based fiber optic biosensor",* Photonics and Nanostructures-Fundamentals and Applications, Vol. 35, No. pp. 100711, (2019).
[16]. K. Setayeshmehr, M. Hashemi, and N. Ansari, *"Photoconversion efficiency in atomically thin TMDC-based heterostructures",* Opt. Express, Vol. 29, No. 21, pp. 32910-32921, (2021).
[17]. Z. Hu, et al., *"Interfacial charge and energy transfer in van der Waals heterojunctions",* InfoMat, Vol. 4, No. 3, pp. e12290, (2022).
[18]. I. Shahbaz, et al., *"Advancements in 2D transition metal dichalcogenides (TMDs) inks for printed optoelectronics: A comprehensive review",* Materials Today, No., (2024).
[19]. C. Cong, et al., *"Optical properties of 2D semiconductor WS2",* Advanced Optical Materials, Vol. 6, No. 1, pp. 1700767, (2018).
[20]. Y. Chen and M. Sun, *"Two-dimensional WS 2/MoS 2 heterostructures: Properties and applications",* Nanoscale, Vol. 13, No. 11, pp. 5594-5619, (2021).
[21]. R. Dutta, et al., *"Optical Enhancement of Indirect Bandgap 2D Transition Metal Dichalcogenides for Multi-Functional Optoelectronic Sensors",* Advanced Materials, Vol. 35, No. 46, pp. 2303272, (2023).
[22]. M. Wang, et al., *"Manufacturing strategies for wafer-scale two-dimensional transition metal dichalcogenide heterolayers",* J. Mater. Res., Vol. 35, No. 11, pp. 1350-1368, (2020).
[23]. Y. Li, et al., *"Measurement of the optical dielectric function of monolayer transition-metal dichalcogenides: MoS 2, Mo S e 2, WS 2, and WS e 2",* Physical Review B, Vol. 90, No. 20, pp. 205422, (2014).

[24]. X. Zhu, et al., *"Effects of dielectric screening on the excitonic and critical points properties of WS 2/MoS 2 heterostructures",* Nanoscale, Vol. 12, No. 46, pp. 23732-23739, (2020).
[25]. H.T. Nguyen, et al., *"Temperature dependence of optical properties of monolayer WS2 by spectroscopic ellipsometry",* Applied Surface Science, Vol. 511, No. pp. 145503, (2020).
[26]. J. Humlíček, *"Polarized light and ellipsometry",* in Handbook of ellipsometry. Springer. p. 3-91, (2005).
[27]. R. Azzam, *"Polarization, thin-film optics, ellipsometry, and polarimetry: Retrospective",* Journal of Vacuum Science & Technology B, Vol. 37, No. 6, (2019).
[28]. B. Von Blanckenhagen, D. Tonova, J. Ullmann, *"Application of the Tauc-Lorentz formulation to the interband absorption of optical coating materials",* Appl. Opt., Vol. 41, No. 16, pp. 3137-3141, (2002).
[29]. L.V. Rodríguez-de Marcos, J.I. Larruquert, *"Analytic optical-constant model derived from Tauc-Lorentz and Urbach tail",* Opt. Express, Vol. 24, No. 25, pp. 28561-28572, (2016).
[30]. D.V. Likhachev, N. Malkova, and L. Poslavsky, *"Modified Tauc–Lorentz dispersion model leading to a more accurate representation of absorption features below the bandgap",* Thin Solid Films, Vol. 589, No. pp. 844-851, (2015).
[31]. X. Ling, et al., *"Parallel stitching of two-dimensional materials",* arXiv preprint arXiv:1512.04492, No. (2015).
[32]. J. Zhang, et al., *"Observation of strong interlayer coupling in MoS2/WS2 heterostructures",* Advanced Materials, Vol. 28, No. 10, pp. 1950-1956, (2016).
[33]. S. Tongay, et al., *"Tuning interlayer coupling in large-area heterostructures with CVD-grown MoS2 and WS2 monolayers",* Nano letters, Vol. 14, No. 6, pp. 3185-3190, (2014).

TÓM TẮT

Nghiên cứu đặc trưng quang học của cấu trúc dị thể 2D MoS_2/WS_2 bằng phương pháp quang phổ ellipsometry

Nghiên cứu này xác định các đặc trưng quang học của cấu trúc dị thể 2D MoS_2/WS_2 bằng phép đo quang phổ ellipsometry (SE) trong dải phổ từ 1,5 đến 6,0 eV với các góc tới khác nhau. Các vật liệu kim loại chuyển tiếp chalcogenide như MoS_2 và WS_2, được biết đến với các tính chất đơn lớp độc đáo, rất lý tưởng cho các ứng dụng quang điện tử. Việc xếp chồng các lớp đơn này làm tăng cường các tính chất có lợi cho việc phát hiện ánh sáng và thu nhận ánh sáng. Phương pháp SE sử dụng mô hình Tauc-Lorentz để phân tích chi tiết, xác định sự hình thành của cấu trúc dị thể TMDC chất lượng cao và đưa ra chính xác các giá trị quan trọng về đặc trưng quang học của vật liệu bao gồm cả phần thực và phần ảo của chiết suất tại từng bước sóng trong khoảng 207 ~ 826 nm (tương đương với năng lượng photon 1,5 đến 6,0 eV). Các giá trị này rất quan trọng để tối ưu hóa các thiết bị quang điện tử dựa trên TMDC cho các ứng dụng quân sự và thương mại.

Từ khoá: Cấu trúc dị thể MoS_2/WS_2; Quang phổ ellipsometry; Mô hình Tauc-Lorentz; Đặc trưng quang học.